Accretion disc dynamics in extreme mass ratio compact binaries

M. R. Truss*
Department of Physics, Durham University, South Road, Durham, DH1 3LE

Abstract

An analysis is presented of a numerical investigation of the dynamics and geometry of accretion discs in binary systems with mass ratios $q = M_2/M_1 < 0.1$, applicable to ultra-compact X-ray binaries, AM CVn stars and very short period cataclysmic variables. The steady-state geometry of the disc in the binary reference frame is found to be quite different from that expected at higher mass ratios. For $q \sim 0.1$, the disc takes on the usual elliptical shape, with the major axis aligned perpendicular to the line of centres of the two stars. However, at smaller mass ratios the elliptical gaseous orbits in the outer regions of the disc are rotated in the binary plane. The angle of rotation increases with gas temperature, but is found to vary inversely with q. At $q = 0.01$, the major axis of these orbits is aligned almost parallel to the line of centres of the two stars. These effects may be responsible for the similar disc structure inferred from Doppler tomography of the AM CVn star GP Com (Morales-Rueda et al. 2003), which has $q = 0.02$. The steady-state geometry at low mass ratios is not predicted by an inviscid, restricted three-body model of gaseous orbits; it is related to the effects of tidal-viscous truncation of the disc near the Roche lobe boundary. Since the disc geometry can be inferred observationally for some systems, it is proposed that this may offer a useful diagnostic for the determination of mass ratios in ultra-compact binaries.

1 Keywords

accretion, accretion discs - binaries: close - novae, cataclysmic variables - instabilities

2 Introduction

2.1 Background

In an interacting binary system, the tidal torque on the accretion disc due to the orbital motion of the secondary star plays two major roles. Firstly, it acts as a sink for the angular momentum that is transported outwards by viscous processes, thereby truncating

*E-mail: m.r.truss@durham.ac.uk

the disc. Secondly, resonances between the orbital motion of the secondary star and the orbital motion of gas in the disc can drive eccentricity growth, precession and spiral waves. Both these processes have a profound impact on the dynamics of the disc and its geometry.

The influence of tides on discs has been studied in great detail for interacting binary systems with mass ratios (defined in this paper as the ratio of the mass of the donor star to the mass of the accreting star) $q \gtrsim 0.1$. The work has been well motivated by the wealth of cataclysmic variables and X-ray binaries that are covered by this range, all with orbital periods of order hours. However, there is a growing body of observational data from ultra-compact systems with orbital periods of the order tens of minutes. These very tight, double-degenerate binaries are often inferred to have extremely small mass ratios. They comprise very low-mass ($M_2 \leq 0.1\mathrm{M}_\odot$), hydrogen-poor donor stars transferring mass onto either a white dwarf (the AM CVn stars), neutron star or black hole (the ultra-compact X-ray binaries). In a recent paper, Deloye, Bildsten & Nelemans (2005) tabulated existing mass ratio determinations for several of the AM CVn systems; these range from $q = 0.087$ for AM CVn itself down to $q = 0.0125$ for CE-315. It is timely, therefore, to revisit the subject of tides with reference to these systems.

2.2 Tides and resonances in accretion discs

Paczyński (1977) calculated orbits in the restricted three-body problem for mass ratios greater than $q \sim 0.03$, and associated the truncation radius of a pressure-free, inviscid disc with the radius of the largest periodic orbit which does not intersect any other periodic orbits. He further found that some large-radius orbits were unstable for mass ratios $q < 0.25$.

Early numerical calculations of viscous discs confirmed that at typical cataclysmic variable mass ratios the disc takes on a steady structure similar to the shape of the inviscid three-body orbits calculated by Paczyński (1977). The disc was found to become slightly elongated perpendicular to the line of centres of the two stars (Whitehurst & King 1991). Furthermore, Whitehurst & King found that their numerical discs became unstable below a critical mass ratio $q_{\mathrm{crit}} \sim 0.25 - 0.33$. They realised the significance of the 3:1 resonance between the orbits of gas in the disc and the orbital motion of the secondary star as a driver for eccentricity generation. This came after previous simulations had shown that superhumps - photometric modulations in the light curve of low mass ratio dwarf novae - could be generated by an eccentric, precessing disc (Whitehurst 1988). Hirose & Osaki (1990) parameterised the resonance condition, showing that the width of the resonance is proportional to the reduced mass of the binary. It follows that the range of resonant radii narrows as q decreases.

Lyubarskij, Postnov & Prokhorov (1994) have confirmed that a circular disc with the standard alpha viscosity is viscously unstable to eccentric perturbations. More recently, Ogilvie (2001) used a viscoelastic theory for turbulent stress to show that the instability can be suppressed by the presence of a large enough relaxation time or bulk viscosity. The theory of tidal instability was refined by Lubow (1991), who highlighted the coupling between the tidal potential and modes excited in the disc on contact with the resonance. Any small existing eccentricity is swiftly amplified, with the growth

rate of the eccentricity proportional to the strength of the two-armed spiral mode. This model, and its application to dwarf nova outbursts has been confirmed many times by numerical simulations (Kunze, Speith & Riffert 1997; Murray 1996, 1998; Truss, Murray & Wynn 2001; Truss 2005).

It is not obvious how the tidal instability manifests itself in systems with very small mass ratios. The growth rate of the instability is proportional to q^2 (Lubow 1991) and hence will be extremely slow, while the range of resonant radii is also extremely narrow (Hirose & Osaki 1990). Simpson & Wood (1998) found precessing, eccentric discs in numerical simulations of binaries with mass ratios $q = 0.05, 0.075$ and 0.1, but *not* in binaries with $q = 0.025$. This suggests that there may be a lower limit below which the instability does not operate, although many more high resolution simulations would be required to verify this.

Recently, there has been renewed interest in the role of the 2:1 resonance at very small mass ratios. Osaki & Meyer (2002) have suggested that the orbital-period photometric humps that appear in the outburst light curves of the low mass-ratio cataclysmic variable WZ Sagittae are caused by the 2:1 resonance. Numerical simulations by Kunze & Speith (2005) have supported this hypothesis.

2.3 Outline of paper

This paper addresses the question of the steady-state structure of an accretion disc in an interacting binary with $q \leq 0.1$. It is shown that the structure of the disc at these mass ratios does not agree with the prediction of an inviscid, three-body model. Rather than taking on a structure that is elongated along an axis perpendicular to the line of centres of the two stars, the disc takes on an elliptical form, offset at an angle to this axis. The angle increases with disc temperature and increases with decreasing q. This effect is related to the tidal truncation of the disc near the Roche lobe. It is not a result of the tidal instability: the analysis presented here refers to discs that have not yet become tidally unstable.

In the next section, the inviscid, restricted three-body model is revisited briefly for systems with low mass ratios. This is followed by a discussion of the results of a series of hydrodynamic simulations of viscous discs. The steady structure of an accretion disc is determined for different mass ratios, and the effect on this structure of different gas temperatures and mass transfer rates is explored.

3 The size of an accretion disc

In the limit of vanishingly small pressure and viscosity, the streamlines of an accretion disc in a binary star potential can be described by periodic orbits in the restricted three-body problem (Lubow & Shu 1975). Paczyński (1977)identified the maximum radius of such a disc with that of the largest simple non-intersecting periodic orbit. Following this methodology, the maximum radius is found by integration of periodic test-particle orbits in the Roche potential. Figure 1 shows the system of coordinates

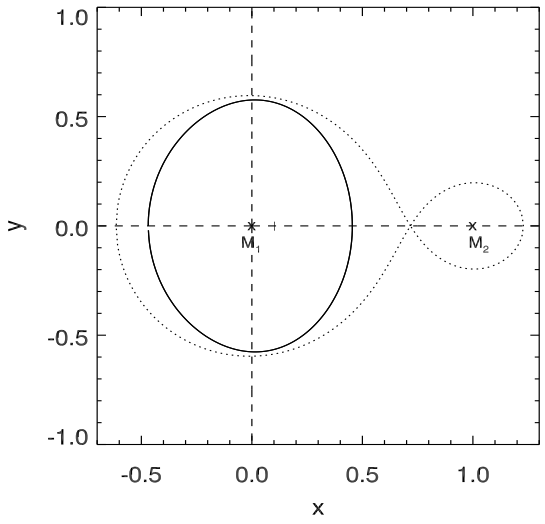

Figure 1: Coordinate system used in the orbit calculations. For reference, the orbit shown here is the last non-intersecting orbit for $q = 0.1$, which has an eccentricity $e = 0.54$. The Roche lobe is also plotted for this mass ratio.

that are adopted. The mass ratio is defined in the modern convention as

$$q = \frac{M_2}{M_1} \tag{1}$$

where the accretion disc is centred on the primary star of mass M_1. This definition is the inverse of that used in Paczyński (1977). The reduced mass is

$$\mu = \frac{q}{1+q}, \tag{2}$$

which here is the distance from the centre of the primary star to the centre of mass (denoted by a short vertical line in Figure 1). Periodic solutions are found by integrating orbits with a given value of the Jacobi constant, and demanding that after one orbit, $x = x(0)$ and $\dot{x} = 0$. The condition $\dot{x} = 0$ ensures that the orbits are symmetric with respect to the x-axis. Furthermore, the stability of the periodic orbits can be investigated following the method of Hénon (1965) and Piotrowski & Ziolkowski (1970). The resulting radii for the last non-intersecting and last stable orbits agree very closely with those tabulated by Paczyński (1977) and Hirose & Osaki (1990), so it is not necessary to reproduce them here. However, it is instructive to show the characteristic shape of these orbits for comparison with later viscous simulations. Figure 2 shows the last non-intersecting and last stable orbits for mass ratios $q = 0.05$ and $q = 0.2$. Their shape is typical of all the last non-intersecting orbits found down to $q = 0.01$: prolate with a high degree of symmetry either side of the line of centres between the two stars (the x-axis in Figure 1). Two other factors were highlighted by this exercise. Firstly, the width

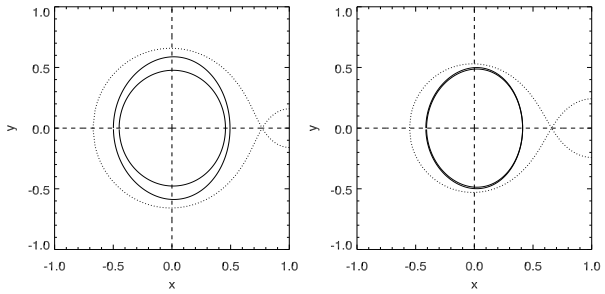

Figure 2: Last stable and last non-intersecting restricted three-body periodic orbits for (a) $q = 0.05$ and (b) $q = 0.2$. The two orbits are very close at $q = 0.2$ as this mass ratio is close to the stability boundary near $q = 0.25$. The Roche lobe for both stars is shown in each case. The origin of the coordinate system is the centre of the primary star, with the centre of the secondary star at $x = 1.0$. Note the high degree of symmetry in the orbits either side of the x-axis.

of the unstable region of orbits was found to decrease with mass ratio, agreeing with the results of Hirose & Osaki (1990). Indeed, the range of unstable orbits becomes so small below $q = 0.02$ that one needs a very accurate integrator to resolve the stability criterion at all.

The second factor relates to the last non-intersecting orbit and is important for a discussion of the truncation of an accretion disc. One can see immediately from Figures 1 and 2 that the maximum radius of these orbits is close to the Roche lobe. This is encouraging, as one naturally expects the Roche lobe to be the absolute maximum radius for retention of a disc, with material outside this radius lost from the system. However, we must not forget that these simple three-body orbits are only appropriate for the completely inviscid case. Real discs are not inviscid; indeed, viscosity plays a crucial role in the transport of angular momentum and thereby in the truncation of an accretion disc. It seems quite possible that for arbitrarily small q, the inviscid three-body model will predict no orbit crossings inside the Roche lobe at all (again, a very accurate integration would be required to prove this beyond doubt). However, it is the presence of a viscosity that breaks the symmetry of the orbits about the line of centres, making the orbits slightly aperiodic and generating the torque required to tidally truncate the disc.

Therefore, the question of whether any of the results from an inviscid calculation can be applied to real discs is something that can only be tested under more physically reasonable conditions. In the next section I present hydrodynamic simulations of viscous accretion discs in order to assess the validity of the three-body approximation to more realistic conditions and to make a systematic investigation of the dynamical response of the disc to different mass injection rates and viscosities.

Run	q	$c_0\,(a\Omega)$	α	$-\dot{M}_2\,(\mathrm{M}_\odot \mathrm{yr}^{-1})$	N	$\theta_{\max}(degrees)$	$e_{\max}$
1	0.01	0.025	0.10	10^{-11}	169634	77	0.57
2	0.03	0.025	0.10	10^{-11}	158992	36	0.55
3	0.10	0.025	0.10	10^{-11}	128414	7	0.59
4	0.01	0.035	0.10	10^{-11}	146443	-	-
5	0.03	0.035	0.10	10^{-11}	139830	55	0.60
6	0.10	0.035	0.10	10^{-11}	109584	17	0.55
7	0.01	0.050	0.10	10^{-11}	105129	$>$90	-
8	0.03	0.050	0.10	10^{-11}	107740	63	0.57
9	0.10	0.050	0.10	10^{-11}	80838	29	0.60
10	0.01	0.035	0.02	10^{-11}	162678	86	0.52
11	0.03	0.035	0.02	10^{-11}	163167	41	0.58
12	0.10	0.035	0.02	10^{-11}	137284	16	0.58
13	0.01	0.035	0.50	10^{-11}	87053	$>$90	-
14	0.03	0.035	0.50	10^{-11}	77120	63	0.57
15	0.10	0.035	0.50	10^{-11}	50551	-	-
16	0.03	0.035	0.10	10^{-13}	139825	57	0.62
17	0.03	0.035	0.10	10^{-9}	139812	52	0.58

Table 1: Data for each simulation. N is the number of particles at the instant of each snapshot in Figures 3, 4 and 5. $\theta_{\max}$ is defined as the tilt angle of the major axis of the outermost disc orbit with respect to the y axis of these plots. $e_{\max}$ is the eccentricity of the outermost disc orbit. The disc in run 15 is no longer in a steady state and has started to precess.

4 Numerical hydrodynamics of accretion discs

4.1 Computational method

The code is a refined version of the three dimensional smoothed particle hydrodynamics (SPH) accretion disc code described by Truss (2005) and references therein (see Monaghan (1992) for a complete review of the SPH technique). The refinement for this work is that the condition of absolute isothermality has been relaxed. While the scheme remains vertically isothermal, the sound speed varies with radius according to:

$$c_{\mathrm{s}} = c_0 R^{-\frac{3}{8}}. \tag{3}$$

where the quantity c_0 is expressed as a fraction of $a\Omega$, where Ω is the orbital angular velocity of the binary and a is the binary separation. The radius R is expressed as a fraction of a. The smoothing length is variable according to the local density and has a maximum value $0.007a$.

4.2 Structural dependence on mass ratio and gas viscosity

A fiducial set of binary parameters was chosen to be representative of ultra-compact binary systems. They were: $M_1 = 0.5\,\mathrm{M}_\odot$, $P_{\mathrm{orb}} = 50\,\mathrm{minutes}$ and $-\dot{M}_2 = 10^{-11}\,\mathrm{M}_\odot \mathrm{yr}^{-1}$.

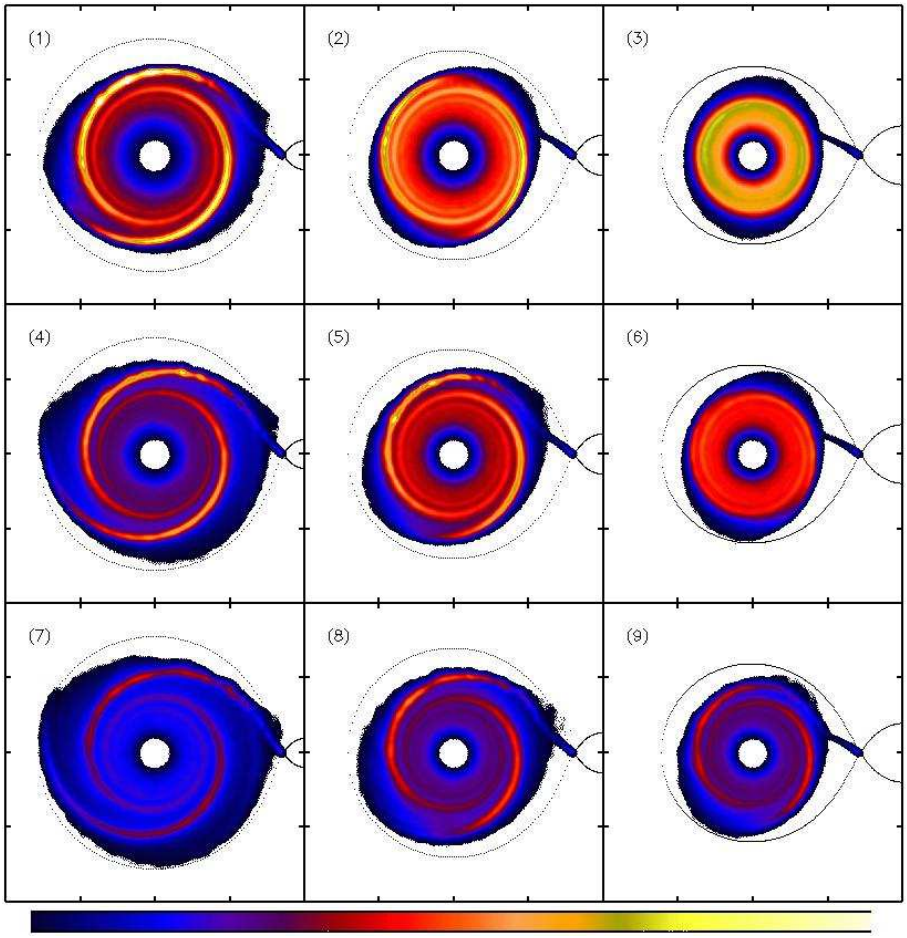

Figure 3: Differences in the surface density structure of an accretion disc according to mass ratio and gas temperature. Each column shows the disc for different gas temperatures at a single mass ratio. Each row shows the variation in structure for different mass ratios at a single gas temperature. The columns from left to right show discs in binaries with $q = 0.01$, $q = 0.03$ and $q = 0.10$ respectively. The rows from top to bottom correspond to $c_0 = 0.025$, $c_0 = 0.035$ and $c_0 = 0.050$ respectively. Labels correspond to the run numbers given in Table 1. The colour scale is normalised such that it is identical for all the discs in Figures 3 and 4. Each box is of side a (one binary separation), with the origin at the centre of the primary star. The Roche lobe is plotted for clarity in each case.

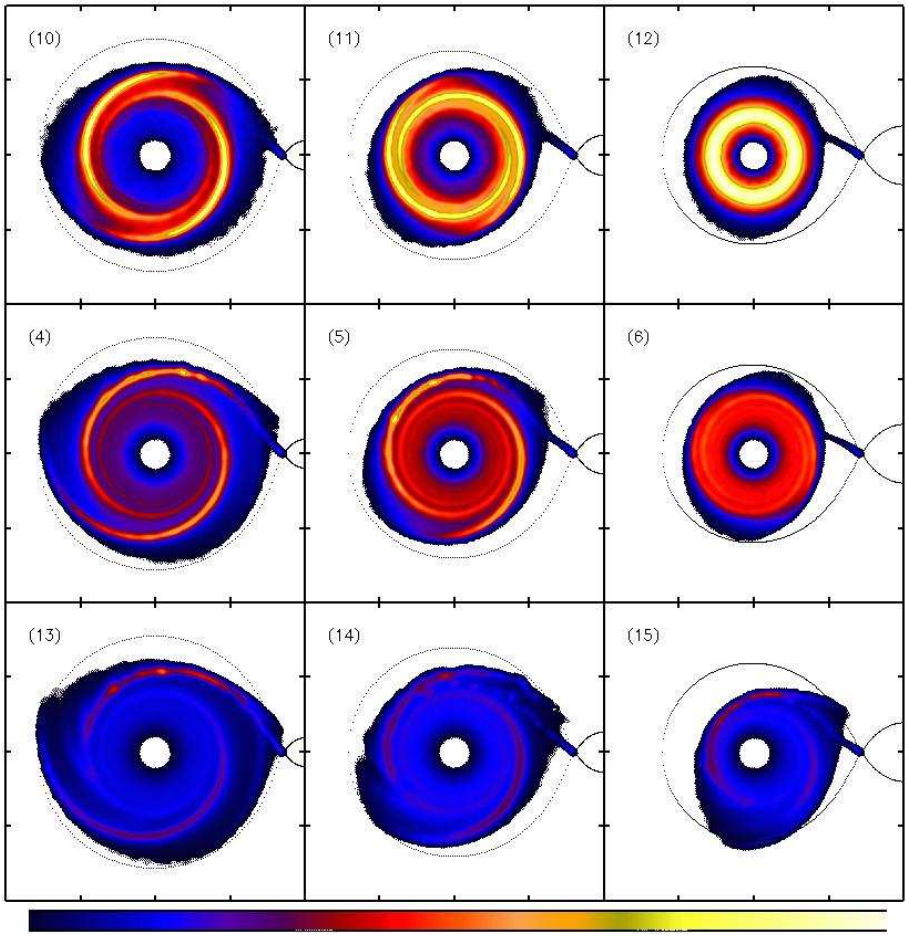

Figure 4: Differences in the steady structure of an accretion disc according to mass ratio and viscosity parameter. Each column shows the disc for different gas temperatures at a single mass ratio. Each row shows the variation in structure for different mass ratios at a single gas temperature. The columns from left to right show discs in binaries with $q = 0.01$, $q = 0.03$ and $q = 0.10$ respectively. The rows from top to bottom correspond to $\alpha = 0.02$, $\alpha = 0.1$ and $\alpha = 0.5$ respectively. Labels correspond to the run numbers given in Table 1: the $\alpha = 0.1$ runs are identical to those shown in Figure 3. Each box is of side a (one binary separation), with the origin at the centre of the primary star. The Roche lobe is plotted for clarity in each case.

In the first set of simulations, a total of nine calculations were performed comprising three disc temperatures at each of three mass ratios, $q = 0.01, 0.03$ and 0.10. The three sound speed parameters used were $c_0 = 0.025$, $c_0 = 0.035$ and $c_0 = 0.050$. For these nine calculations, the Shakura/Sunyaev viscosity parameter was set to $\alpha = 0.1$. The temperatures at the outer edge of the disc that the sound speeds correspond to depend weakly on the binary parameters for each simulation, but as a guide if $q = 0.01$, $c_0 = 0.025$ corresponds to a mid-plane temperature of about $25,000\,\mathrm{K}$ (for $\mu = 1$). A second set of calculations was performed to investigate the dependence of the disc structure on the Shakura/Sunyaev viscosity parameter. These calculations comprised six further runs with $\alpha = 0.02$ and $\alpha = 0.5$ at each mass ratio, all with $c_0 = 0.035$, to complete a similar 3×3 grid of calculations in $q - \alpha$ space. Table 1 summarises the input parameters for these and the further simulations described in this paper, together with information regarding the number of particles involved for each run.

Each disc was built up in three dimensions from scratch, injecting SPH particles from the L_1 point at the correct angle to the line of centres prescribed by Lubow & Shu (1975). The discs were allowed to evolve in this way and settle to a steady, circularised state in which the total eccentric mode strength had ceased to decline. This is an important criterion to satisfy, as during the initial stages of disc formation the total eccentric mode strength is high. The mode strength decreases as the disc material is circularised and spreads under the action of viscosity. After it reaches a minimum value, the disc will either continue to remain circular, or become eccentric if parts of it can access the 3:1 resonance. All but one of the discs described here are fully circularised, with eccentric mode strengths in the range $10^{-4} < S(1,0) < 5 \times 10^{-3}$ (the exception, run 15, is discussed below). The time taken to achieve this fully circularised state corresponds to many tens of orbital periods, or many thousands of dynamical times of the disc. As a benchmark guide, the mode strength must reach several times 10^{-3} to produce even the tiniest amount of disc precession (Truss 2005). Therefore it can be stated with certainty that these discs are well developed, but not tidally unstable. This does not preclude them from becoming tidally unstable given an indefinite amount of time to evolve; the growth rate of the instability is, as we have seen previously, extremely slow.

Figure 3 shows the results of the first nine simulations. It can be seen immediately that the steady shape of the disc fixed in the binary frame is, in general, not that suggested by the shape of the restricted three-body orbits. As mass ratio decreases, or as sound speed increases, the major axis of the elliptical orbits in the outer parts of the disc becomes rotated in the x-y plane. The closest approximation to the shape predicted by the restricted three-body orbits (and previous calculations of discs in binaries with larger mass ratios) is that shown for run 3 in Figure 3 ($q = 0.10$ and $c_0 = 0.025$). The major axis for this disc is aligned nearly perpendicular to the line-of-centres. However, we can see that the disc in run 1, which has a similar temperature to that in run 3 but has $q = 0.01$, is quite different. The major axis of this disc is aligned nearly parallel to the line-of-centres.

The rotation angle, $\theta_{\max}$, is defined as the tilt angle between the major axis of the outermost disc orbit and the line perpendicular to the line-of-centres. The maximum

eccentricity is defined here as

$$e_{\max} = \sqrt{\left(1 - \frac{b^2}{a^2}\right)} \tag{4}$$

where a and b are the semi-major and semi-minor axes of the outermost disc orbit. These quantities are summarised in Table 1.

Further inspection of Figure 3 reveals that the rotation angle of the orbits is correlated strongly with the distance from the disc edge to the L_1 point (or the length of the mass transfer stream). A hotter disc spreads further under the action of viscosity, while the smaller the mass ratio, the larger the fraction of the Roche lobe of the primary star that can be populated by stable orbits. There is little variation in maximum eccentricity of the discs, with a mean value $< e_{\max} >= 0.58$ and a standard deviation $\sigma = 0.03$.

It is noteworthy that the spiral arms become less tightly wound for hotter discs as one would expect, but the same effect is also seen for discs in binaries with smaller and smaller mass ratios. In all cases, the spiral arms are confined within the Roche lobe of the primary star. The structure of the hot discs at $q = 0.01$ (runs 4 and 7) is complex, showing asymmetry in both the x- and y- directions. At this mass ratio and these temperatures, the orbits are no longer elliptical, so no value of $e_{\max}$ can be ascribed to them. The mass transfer stream can be seen joining the near-side spiral arm very close to the L_1 point. Indeed, the disc extends out to the Roche lobe boundary across a wide range of azimuth in these discs, and there was a significant rate of mass loss from the disc edge in these simulations. A similar situation may occur in discs around weakly magnetised white dwarfs, where the outer edge of the disc is propelled outwards by the magnetic field. Matthews et al. (2006) have discussed the implications of this mass loss (in the case of a magnetised primary) for our understanding of binary star evolution.

Figure 4 shows the results of the second set of simulations (runs 10-15), in which the gas viscosity parameter was varied at each mass ratio. Runs 4-6 are reproduced in Figure 4 to aid comparison. Again, the values derived for $\theta_{\max}$ and $e_{\max}$ are summarised in Table 1. The results are very similar to those in Figure 3, with the expected trend of increasing $\theta_{\max}$ with viscosity parameter. There is one notable exception, however. Run 15 (q = 0.10, c_0 = 0.035 and $\alpha = 0.5$) is no longer in a steady state and has started to precess. The viscous spreading at this α is very rapid and the disc edge quickly encounters the 3:1 resonance. However, even though the thermal characteristics of the discs in runs 13 and 14 are identical (they differ only in mass ratio), neither of those discs is close to finding a state of precession. This is a direct demonstration that the growth rate of the tidal instability is very slow at small mass ratios: having encountered the resonance, these discs need much longer to start precessing.

4.3 Structural dependence on mass transfer rate

A further parameter that is known to influence the shape of an accretion disc is the magnitude of the mass transfer rate from the companion star. The stream is a constant source of low specific angular momentum material, and this can act to circularise the

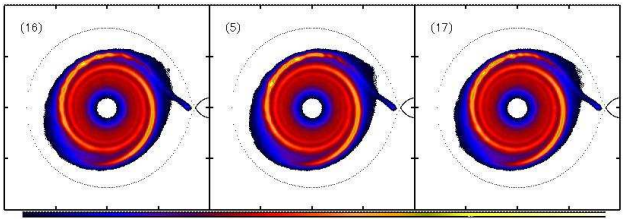

Figure 5: The effect of varying the mass injection rate on disc structure for $q = 0.03$. From left to right, the mass transfer rates are $\dot{M} = 10^{-13}\,\mathrm{M}_{\odot}\mathrm{yr}^{-1}$, $\dot{M} = 10^{-11}\,\mathrm{M}_{\odot}\mathrm{yr}^{-1}$ (run 5) and $\dot{M} = 10^{-9}\,\mathrm{M}_{\odot}\mathrm{yr}^{-1}$ respectively. The particle mass in each simulation is scaled from the mass transfer rate; the surface densities in runs 16 and 17 are therefore 1/100th and 100 times those in run 5.

gaseous orbits (Lubow 1994). It is important, therefore, to investigate this effect for the systems with $q \leq 0.1$ that are under study here.

The simulation for $q = 0.03$, $c_0 = 0.035$ and $\alpha = 0.1$ (run 5) was repeated using mass injection rates of 10^{-9} and $10^{-13}\,\mathrm{M}_{\odot}\mathrm{yr}^{-1}$. The results are shown alongside the original $10^{-11}\,\mathrm{M}_{\odot}\mathrm{yr}^{-1}$ run for comparison in Figure 5. While there is a weak trend for decreasing eccentricity and rotation angle with increasing mass transfer rate, the effect on the geometry of the steady disc at different mass transfer rates is not dramatic. It should be noted that this situation, in which each disc is built from scratch with a steady mass-transfer rate, is quite different from that in which a disc is subject to an instantaneous enhancement or interruption in mass transfer (see for example, Murray, Warner & Wickramasinghe (2000)).

4.4 Other considerations

The rotation angles and eccentricities derived in this work are determined using the outermost edge of the accretion disc, where the surface density can be low. It is instructive, therefore, to investigate briefly the effect on the disc structure of neglecting the lowest density regions. Figure 6 shows the effect of removing regions with less than 10% and 20% of the maximum surface density in representative simulations for q = 0.01 (run 4) and q = 0.10 (run 6). It is immediately clear that this does have some effect on the inferred structure, especially at q = 0.10. In this case, the rotation angle disappears and the eccentricity falls at the 10% level and the disc appears completely circular at the 20% level. At q = 0.01, a large rotation angle and eccentricity are still measurable at the 10% level, but things become less clear at the 20% level. Here, the main body of the disc is circular apart from the trailing ends of the two spiral arms.

It is also important to examine the difference in the inferred structure if we map the viscous energy dissipation rate in the disc rather than the surface density. This may offer a better comparison with observational tomographic techniques which map disc emission. Figure 7 shows the two quantities mapped onto the disc for q = 0.03 (run 5). While there is not necessarily a strong correlation between regions of high emission and regions of high surface density - the extended stream impact hot-spot is a good example

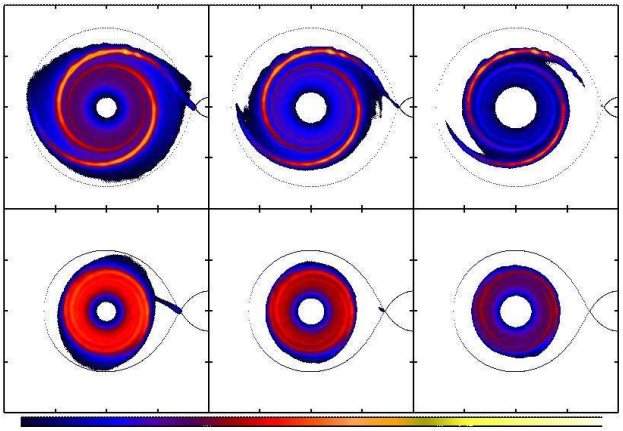

Figure 6: The effect of neglecting low surface-density regions of the disc. The rows correspond to run 4 (q = 0.01, top) and run 6 (q = 0.10, bottom). The left-hand panel shows the entire disc structure, while in the centre and right-hand panels, the lowest 10% and 20% of the surface density have been removed respectively.

- the measured rotation angle and eccentricity are consistent for both quantities. Indeed, this is a general result for all the simulations presented here. However, it should be noted when comparing with observations that Doppler tomograms are reconstructed from single emission lines and that these lines are produced in different regions of the accretion disc according to the local conditions.

5 Discussion

It has been shown that for mass ratios $q = \frac{M_2}{M_1} \leq 0.1$, the steady-state geometry of the disc in the binary frame is found to be quite different from that expected at higher mass ratios. For $q \sim 0.1$, the disc takes on the usual elliptical shape, with the major axis aligned perpendicular to the line of centres of the two stars. However, at smaller mass ratios the elliptical gaseous orbits in the outer regions of the disc are rotated, with the major axis inclined in the direction of the secondary star. At $q = 0.01$, the major axis of these orbits is aligned almost parallel to the line of centres of the two stars. The rotation is more pronounced in hot, viscous discs, though there is no apparent correlation with the rate of mass transfer from the donor star.

The key ingredient in determining the magnitude of the rotation angle is the maximum radius of the accretion disc and, in particular, the distance from the inner Lagrangian point to the disc edge. The disc occupies a large fraction of the Roche lobe at small mass ratios and the L_1-disc distance can be small. Furthermore, a hot disc spreads further under the action of viscosity than a cool disc.

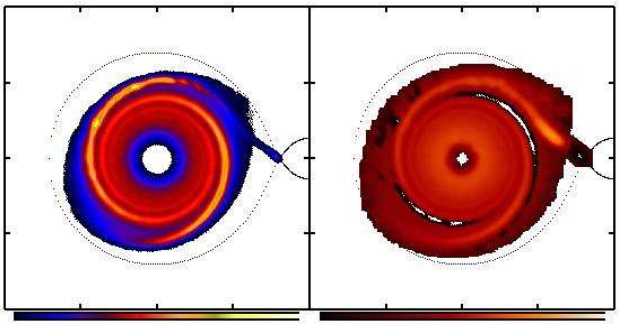

Figure 7: A comparison of surface density structure (left) and energy dissipation rate (right) for run 5 (q = 0.03). Both quantities yield consistent results for the angle $\theta_{\max}$ and the maximum eccentricity. High density regions do not necessarily correspond to regions of large emission: note the extended impact hot spot and the regions of very low emission just behind the spiral arms.

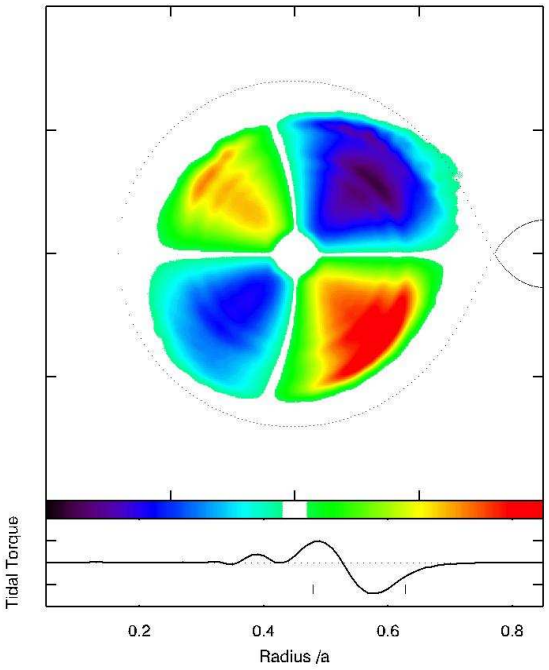

Figure 8: Tidal torques on an accretion disc for $q = 0.03$, showing the alternating quadrants of positive (green to red) and negative (black to blue) torques. The lower panel is an azimuthally-averaged radial torque profile (with arbitrary units of torque) and shows that the averaged contribution is only significant in the outer regions of the disc. The theoretical positions of the 3:1 and 2:1 resonances are marked by short vertical lines.

5.1 Tidal truncation radii

It is clear that there is some value in being able to make a reliable estimate of the maximum radius of an accretion disc. In the absence of any other significant torques (for example, a strong stellar magnetic field anchored on the primary star), the disc is truncated by the tidal interaction with the secondary star, somewhere inside the Roche lobe boundary. The tidal/viscous truncation radius can only be determined numerically (Frank, King & Raine 2002), so a fully three-dimensional hydrodynamical model such as the one discussed here provides an ideal tool. Figure 8 shows the tidal torque field across the accretion disc for a binary system with $q = 0.03$. The alternating quadrants of positive and negative torque described by Frank, King & Raine (2002) are clearly visible and the benefit of modern computer power allows the resolution of a wealth of detail associated with the spiral structure in the disc. The lower panel of Figure 8 shows the radial profile of azimuthally-averaged torque. The net torque contribution is negligible in the inner parts of the disc, but very significant where the spiral arms are most prominent in the outer parts. This result supports the findings of Blondin (2000), who found that the angular momentum transport in a disc due to tidal torques was not significant in the inner regions, but large near the disc edge (driving an effective viscosity parameter $\alpha \sim 0.1$).

Frank, King & Raine (2002) associate the tidal radius of the disc with the point at which the torque first changes sign; in the case of Figure 8 this is near $R = 0.52a$. However, for discs which deviate from azimuthal symmetry, it is clear that a single radius does not describe the geometry of the disc fully. This certainly will be the case for discs in binaries with small mass ratios. In the example shown here, for $q = 0.03$, the disc radius varies with azimuth from $R = 0.54a$ to $R = 0.68a$. It remains true that the estimate

$$\frac{R_{\rm tide}}{a} \simeq 0.9 R_1 \tag{5}$$

(Frank, King & Raine (2002)), where R_1 is the radius of the primary Roche lobe, is representative of the *average* radius of the disc. For $q = 0.03$, this gives $R_{\rm tide} = 0.6$a, with $\sim 10\%$ variation over the full range of radii.

5.2 Application to GP Com and other ultra-compact binaries

The predicted shape of the accretion disc at low mass ratio - elliptical and fixed in the binary frame at an angle to the line-of-centres - has been observed in the AM CVn system GP Com, which has an orbital period of 46 minutes and has a mass ratio $q \sim 0.02$ (Marsh 1999). Morales-Rueda et al. (2003) found that the He I emission in Doppler tomograms of GP Com had elliptical rather than circular symmetry. Fits to equal flux contours were found to be ellipses with a maximum eccentricity $e \sim 0.6$. The ellipses are not aligned perpendicular to the line-of-centres (Figure 7 of Morales-Rueda et al. 2003). Morales-Rueda et al. (2003) have suggested that the discrepancy between their observation and the predictions of the restricted three-body model may indicate an error in the ephemeris of GP Com. However, the simulations described in this paper suggest that no such problem exists. Although the observed geometry of the disc disagrees with the inviscid three-body model, it is entirely consistent with the

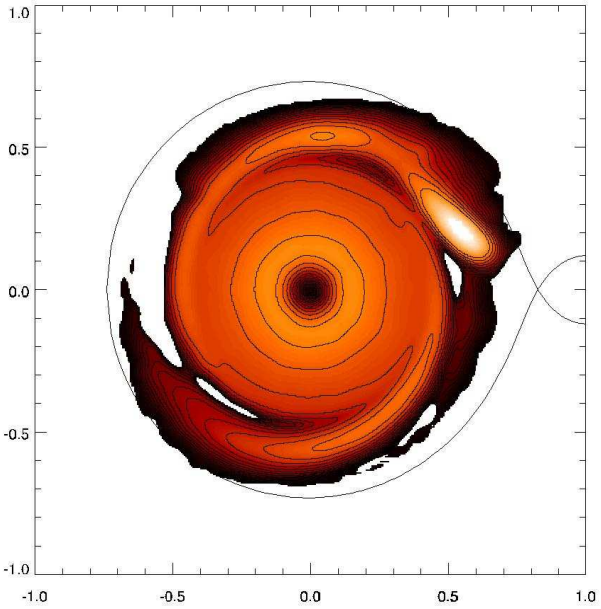

Figure 9: Contours of energy dissipation rate per unit area in a disc with $q = 0.02$. The contours of constant dissipation are circular in the inner parts of the disc but elliptical in the outer parts. The stream-impact hot-spot is clearly visible. The colour scale is logarithmic, running from $10^5\,\mathrm{erg\,s^{-1}cm^{-2}}$ (darkest shade) to $10^{11}\,\mathrm{erg\,s^{-1}cm^{-2}}$ (lightest shade).

predictions of a three-dimensional, viscous hydrodynamic model which includes the effects of mass transfer.

Figure 9 shows the contours of total energy dissipation rate per unit area in a simulation of a disc in a binary with $q = 0.02$. The emission contours from the inner regions of the disc are circular, while those from the cooler, outer disc are broadly elliptical, with some sub-structure associated with the hot spot and spiral arms. The angle of these elliptical contours from the normal to the line-of-centres of the two stars is about 40 degrees. The ratio of the semi-minor to semi-major axes of the outer orbits is 0.83, giving an eccentricity $e = 0.55$. These results compare favourably with the geometry of GP Com inferred from the Doppler maps of Morales-Rueda et al. (2003).

Since the angle is expected to vary for different mass ratios, its measurement may be a useful diagnostic for the determination of mass ratios in very short period binaries. The angle does not specify q absolutely uniquely; for example, it can be seen from Figure 3 that the tilt angle for $q = 0.03$ and $c_0 = 0.025$ (run 2) is similar to that for $q = 0.1$ and $c_0 = 0.05$ (run 9). However, if more information is available, or if reasonable assumptions can be made regarding the temperature of the disc, then the angle can be associated with a narrow range of possible mass ratios. Furthermore, for $q \lesssim 0.01$, the disc geometry is unique and fairly independent of temperature.

6 Concluding Remarks

The use of measurements of the rotation angle of an accretion disc to place constraints on the binary mass ratio should represent a useful diagnostic that can be used hand-in-hand with spectroscopic determinations. Further Doppler tomography of ultra-compact systems is required to verify the predictions of the hydrodynamical models discussed here: the model will stand or fall by these new observations. It will be particularly interesting to see if the asymmetrical disc geometry predicted for discs in binaries with $q \sim 0.01$ is found observationally. The smallest ultra-compact binary mass ratio claimed so far is $q = 0.0125$ for CE-315 (Deloye, Bildsten & Nelemans (2005), though Ruiz et al. (2001) have cited $q = 0.022$). No Doppler maps have appeared in the literature thus far for this system.

The independence of disc geometry on mass injection rate is slightly surprising and this should be a focus of future theoretical work. The thermal properties of the gas in the stream-impact region are known to affect the extent to which the stream can overflow the disc edge (Armitage & Livio 1998). It is conceivable that the inclusion of full radiative transfer in the hot-spot region will lead to discs with slightly different radii. Further theoretical work on the behaviour of the tidal instability at these very low mass ratios is also desirable. It is of particular importance to find out whether the instability is suppressed completely below a critical threshold value of q. While we know that the resonance can be identified in an inviscid 3-body model down to mass ratios far smaller than those discussed here, we do not know whether this will translate into a viable instability in a viscous disc in a binary with $q \sim 0.01$. It can be seen from Figures 3 and 4 that the disc at q = 0.01 already fills most of the Roche lobe long before any measurable precession is detected. It is not clear at all how any subsequent precession could be maintained: inevitably there would be significant mass loss across the Roche lobe boundary.

The steady state geometry of discs in extreme mass ratio systems predicted by this work is an example of a physical situation in which the inviscid, restricted three-body model breaks down when applied to accretion discs. Failures of the model are surprisingly rare. The last non-intersecting three-body orbit remains a good estimate of the tidal truncation radius for $q > 0.1$, while the critical upper limit for tidal instability at $q = 0.25$ in the three-body problem agrees well with both observations of cataclysmic variables and previous numerical calculations. However, at $q < 0.1$, the disc can fill a very large fraction of the Roche lobe. The presence of a non-zero viscosity coupled with the action of the tides leads to a strong, asymmetric torque on the gas, as shown in Figure 8. The asymmetry is most pronounced for the largest orbits, and it is this that leads to the rotation of the orbits away from the perpendicular to the line-of-centres.

Acknowledgements

This work was instigated during a visit to the Centre for Astrophysics and Supercomputing at Swinburne University of Technology in Melbourne in late 2005. I would like to thank them, and in particular James Murray for their hospitality during my stay. I am also grateful to Gordon Ogilvie for a helpful discussion about the characteristics of

the tidal instability and to the anonymous referee for several constructive comments.

Bibliography

Armitage P., Livio M., 1998, ApJ, 493, 898
Blondin J.M., 2000, New Astron., 5, 53
Deloye C.J., Bildsten L., Nelemans G., 2005, ApJ, 624, 934
Frank J., King A.R., Raine D.J., 2002, Accretion Power in Astrophysics, 3rd edn. Cambridge University Press
Goodchild S., Ogilvie G., 2006, MNRAS, 368, 1123
Hénon M., 1965, Ann. d'Ap, 28, 992
Hirose M., Osaki Y., 1990, PASJ, 42, 135
Kunze S., Speith R., 2005, The Astrophysics of Cataclysmic Variables and Related Objects, eds. Hameury J.-M., Lasota J.-P., ASP Conference Series, 330, 389
Kunze S., Speith R., Riffert H., 1997, MNRAS, 289, 889
Lubow S.H., 1991, ApJ, 381, 259
Lubow S.H., 1994, ApJ, 432, 224
Lubow S.H., Shu F.H., 1975, ApJ, 198, 383
Lyubarskij Y.E., Postnov K.A., Prokhorov M.E., 1994, MNRAS, 266, 583
Marsh T.R., MNRAS, 304, 443
Matthews O.M., Wheatley P.J., Wynn G.A., Truss M.R., 2006, MNRAS, 372, 1593
Monaghan J.J., 1992, ARA&A, 30, 543
Morales-Rueda L., Marsh T.R., Steeghs D., Unda-Sanzana E., Wood J.H., North R.C., 2003, A&A, 405, 249
Murray J.R., 1996, MNRAS, 279, 402
Murray J.R., 1998, MNRAS, 297, 323
Murray J.R., Warner B., Wickramasinghe D.T., 2000, MNRAS, 279,402
Ogilvie G.I., 2001, MNRAS, 325, 231
Osaki Y., Meyer F., 2002, A&A, 383, 574
Paczyński B., 1977, ApJ, 216, 822
Piotrowski S.L., Ziolkowski K., 1970, Ap&SS, 8, 66
Ruiz M.T., Rojo P.M., Garay G., Maza J., 2001, ApJ, 552, 679
Simpson J.C., Wood M.A., 1998, ApJ, 506, 360
Truss M.R., 2005, MNRAS, 356, 1471
Truss M.R., Murray J.R., Wynn G.A., 2001, MNRAS, 324, L1
Whitehurst R., 1988, MNRAS, 233, 705
Whitehurst R., King A.R., 1991, MNRAS, 249, 25